

Elemental Phosphorus: structural and superconducting phase diagram under pressure

José A. Flores-Livas^{1,*}, Antonio Sanna², Alexander P. Drozdov³, Lilia Boeri⁴, Gianni Profeta⁵, Mikhail Erements³, and Stefan Goedecker¹

¹Department of Physics, Universität Basel, Klingelbergstr. 82, 4056 Basel, Switzerland

²Max-Planck Institut für Mikrostruktur Physik, Weinberg 2, 06120 Halle, Germany

³Max-Planck Institut für Chemie, Chemistry and Physics at High Pressures Group Postfach 3060, 55020 Mainz, Germany.

⁴Institute of Theoretical and Computational Physics, Graz University of Technology, NAWI Graz, 8010 Graz, Austria

⁵Dipartimento di Fisica Università degli Studi di L'Aquila and SPIN-CNR, I-67100 L'Aquila, Italy

*jose.flores@unibas.ch

ABSTRACT

Pressure-induced superconductivity and structural phase transitions in phosphorous (P) are studied by resistivity measurements under pressures up to 170 GPa and fully *ab initio* crystal structure and superconductivity calculations up to 350 GPa. Two distinct superconducting transition temperature (T_C) vs. pressure (P) trends at low pressure have been reported more than 30 years ago, and for the first time we are able to reproduce them and devise a consistent explanation founded on thermodynamically metastable phases of black-phosphorous. Our experimental and theoretical results form a single, consistent picture which not only provides a clear understanding of elemental P under pressure but also sheds light on the long-standing and unsolved *anomalous* superconductivity trend. Moreover, at higher pressures we predict a similar scenario of multiple metastable structures which coexist beyond their thermodynamical stability range. Metastable phases of P experimentally accessible at pressures above 240 GPa should exhibit T_C 's as high as 15 K, i.e. three times larger than the predicted value for the ground-state crystal structure. We observe that all the metastable structures systematically exhibit larger transition temperatures than the ground-state ones, indicating that the exploration of metastable phases represents a promising route to design materials with improved superconducting properties.

Introduction

The discovery that sulfur hydride (SH_3) is superconductor with a record-breaking critical transition temperature (T_C) of 200 K¹, has disproved a decades-long prejudice against high- T_C occurring conventionally^{2,3}. This result demonstrated that extreme pressures represent a novel avenue to access new physical phenomena and exotic states of matter, which in the next years may lead to many surprises. Sulfur hydride is not an isolated example of conventional high- T_C superconductivity at high pressures, since a few months later also phosphine (PH_3) has been observed to superconduct at transition temperatures as high as 100 K at 200 GPa⁴.

The case of phosphine it is even more fascinating than that of SH_3 , whose crystal structure and superconducting phase diagram have been largely studied and unambiguously determined both experimentally^{8,9} and theoretically^{10–17}. In fact, the same theoretical methods which were used successfully to predict SH_3 , show that at high pressure PH_3 should decompose into its elemental components, phosphorus and hydrogen. Since the *ab-initio* description of the thermodynamics of hydrides is in general quite accurate, the most likely explanation is that the reported superconducting phase of PH_3 is to occur in a *metastable* structure of PH_n ($n = 1, 2, 3, 4$) stabilized by a particular, nevertheless reproducible experimental condition^{18,19}.

Metastable phases, which can be accessed only under specific thermodynamical conditions, play a major role in determining the high pressures properties in many compounds; in some cases, they can lead to complicated superconducting phase diagrams, even for simple elements²⁰.

The most prominent example is hydrogen, where the search for a possible metallic phase²¹, which could be a room-temperature superconductor²² has been going on for decades. Actual hints for metalization have been recently reported in Ref.²³ and were based on the temperature dependence of electrical resistance and disappearance of Raman spectra. However the reported metallization in Ref.²⁴ observed for atomic hydrogen based on reflectance of the sample is still debated^{25–27}. What is certain is that the metallic phase involves metastable phases that are only accessible at high pressures and precise temperatures^{23,28–30}.

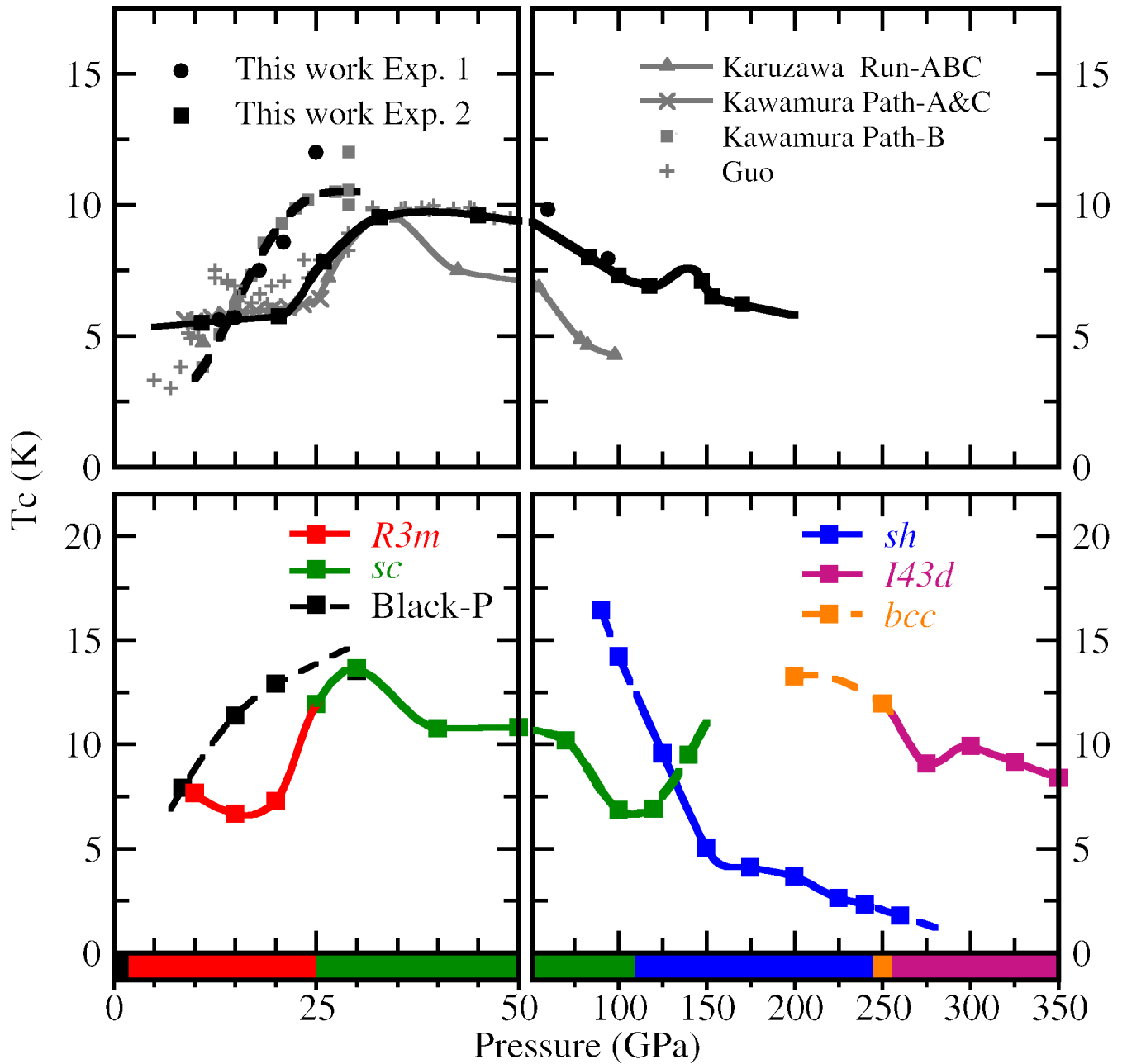


Figure 1. Summary of all the critical temperatures observed experimentally⁵⁻⁷ (top panels) and calculated theoretically in this work (bottom panels). In the experimental panels the dashed and full lines are a guidelines-to-the-eye and used to distinguish the trend that we interpret as due to metastable black-P (dashed) from the energetically stable sequence of transformations (see text). The color-bar at the bottom indicates the sequence of calculated ground-state structures; the color-code is explained in the legend of the bottom panels.

Although less spectacular in terms of critical temperature, phosphorus is another well-known example of elemental compound, which becomes superconducting under pressure and has a rich and complicated phase diagram³¹.

In this work, we present a thorough investigation of the superconducting properties of phosphorus under pressure, including new experiments at high pressure and, for the first time, a fully *ab-initio* characterization. We discovered that the structural metastability of phosphorus plays a crucial role in determining the superconducting phase diagram and unquestionably this is driven by pressure and temperature conditions. Thanks to our *ab-initio* study we were able to disentangle the nature of the superconducting properties of P metastable phases and more importantly to predict that these phases have larger transition temperatures than the putative ground state ones.

Results

High-pressure Experiments

The superconducting phase diagram of P is intriguingly complicated; the top panel of Fig. 1 compares the previous experimental results (gray symbols and lines) with our new experiments (black symbols and lines). The first accurate resistivity measurements on P under compression date back to 1985 and were performed by Kawamura *et. al.*⁵. The authors reported for the first time an *anomalous* behavior in the superconducting transition temperatures up to pressures of 30 GPa: the value of T_C was found to strongly depend on the $P - T$ path followed in experiment. The problem was revisited by Karuzawa *et. al.*⁶ in early 2000's, with a second set of experiments in which transition temperatures were measured for pressures of up to 97 GPa, producing a single T_C trend. More recently Guo *et. al.*⁷ carried out Hall-electrical measurements under pressure up to 50 GPa, and reported a non-monotonic trend of T_C at low pressures, and an anomaly due to a Lifshitz transition at ~ 17 GPa.

Clearly, despite the effort and several experiments over decades, the explanation of the superconducting trends and more importantly the anomalous dependence on thermodynamic conditions remains unsolved. Given the polymorphism of elemental phosphorus already at ambient conditions, one could speculate that the anomalous T_C vs. P trends are caused by the coexistence of metastable phases. Therefore, in the present work we design two different sets of experiments which specifically aim at accessing different phases (stable and metastable) following two $P - T$ thermodynamic paths, as schematically illustrated in top panels of Fig. 2.

In the first set, Exp. 1, (the measured T_C is reported as black circles in the top panel of Fig. 1) the sample is constantly kept at low temperature while pressure is increased. In the second $P - T$ path (Exp. 2) the temperature is raised at higher temperatures when applying pressure and for resistivity measurements. In this figure bottom panels show the resistivity measurements at different pressures and T_C 's are indicated with arrows. Clearly the T_C vs. P behavior of the two datasets is rather different. In the first set (black circles in Fig. 1) a slow increase of T_C up to 25 GPa is observed, while for the second set of experiments T_C sharply increases with pressure (black squares in Fig. 1). The two data sets merge at 25 GPa, and a single trend is observed up to the highest common pressure measured (94 GPa).

Ab-initio Phase diagram of P under pressure

Fig. 3 shows the computed enthalpy for different allotropes of phosphorus under pressure found using our crystal structure prediction method. The enthalpy difference is shown with respect the *sc* ($Pm - 3m$) phase. The lowest-enthalpy sequence of transitions, according to the calculations, is the following: Red-P (triclinic $P - 1$)³² is stable at 0 GPa and almost degenerate with black-P (*Cmca*)³³, which is the experimentally observed phase; phase *P - II* ($A7-R3m$) occurs from 3 to 16 GPa. The simple cubic (*sc-P - III*) lattice dominates for pressures up to 120 GPa, where the simple hexagonal lattice (*sh-P6mmm*) is stable up to ~ 225 GPa. We find the *bcc* ($Im - 3m$) crystal stable from 225 to 250 GPa and finally the last phase ($I - 43d$) is stable from 250 to beyond 350 GPa. The sequence of transitions is shown as a color bar at the bottom of Fig. 1.

The three relevant pressure intervals, in which phase transitions take place, are highlighted in top panels of Fig. 3. The first one (left) shows the low-pressure regime. At ambient conditions phosphorus is known in at least three different allotropic forms: black-P, red-P and white-P. Experimentally, black-P is the most stable form³³ which transforms to the *A7* phase³⁴ for pressure above 5 GPa³⁵. In our calculations, red-P is the ground state at zero pressure (although is almost degenerate with black-P), while the stabilization energy of white-P is 130 meV per atom higher (or equivalently ~ 1500 K). The apparent disagreement is due to the fact that the standard Generalized Gradient Approximation (GGA) functional used in this work is inaccurate for layered (van-der-Waals bonded) or polymeric systems in predicting the exact structural sequence for different polymorphisms. However, although the Van-der-Waals interaction is rather important in the very low-pressure region of the phase diagram (0-5 GPa), it plays only a minor role at higher pressures, where superconductivity occurs. We find that black-P remains enthalpically competitive within a comparable order-of-magnitude (~ 0.1 eV) with other low-enthalpy phases up to pressures as large as 30 GPa. As will be discussed in detail in the next section, the meta-stability of this phase turns out to be fundamental to describe the experimental trend in T_C .

The second panel (top central) of Fig. 3 shows the pressure interval in which the *sh* \rightarrow *bcc* transition occurs. In this window *sc*, *sh* (*P6mmm*), *IM-Cmmm* (not shown), *bcc* and, surprisingly, black-P (in a collapsed form) are structures that are all accessible within a few tens of meV energy difference. This enthalpy landscape is consistent with experimental evidences that in this pressure range the *sh* \rightarrow *bcc* transition occurs via an intermediate incommensurate phase³⁶.

A third pressure range, worth analyzing in more detail (top right panel), is where the *sh* and *bcc* enthalpy curves cross each other and the *bcc* to $I - 43d$ transformation occurs ($I - 43d$ is a distorted form of *bcc*). Note that in this case the enthalpy differences between all three phases are extremely small, i.e. within the computational accuracy, so that vibrational entropy corrections (not included) and stabilization of distorted complex structures^{34,37} could in principle affect the energetic ranking of the structures and the transition pressures. However, these corrections will shift the transition pressure by no more than ~ 5 GPa, which is below the experimental errors to estimate the pressure (~ 10 GPa).

Indeed, our *ab initio* zero-temperature phase diagram is in substantial agreement with the sequence experimentally

observed^{34–36,38–43}, and is therefore a good starting point to calculate the superconducting critical temperatures as a function of the pressure. Furthermore, our analysis has allowed us to characterize several of the structural transitions as first-order, i.e. with a discontinuous $P(V)$ behaviors (see Fig. 4); this could lead to a possible path to stabilize metastable structure under suitable thermodynamic conditions.

Ab-initio predicted superconducting temperatures

Using state-of-the-art Density Functional Theory for Superconductors (SCDFT) combined with density-functional perturbation theory for the calculation of phonon dispersions and electron-phonon coupling and linear response theory in the random phase approximation for the evaluation of electron-electron repulsion, we have computed the superconducting properties (anomalous density and critical temperature, T_C) for all the identified structures of P which are dynamically stable. The corresponding T_C 's are shown in the lower panel of Fig. 1, as full (dashed) lines for ground-state (metastable) structures.

Low Pressures (0-50 GPa) As shown in the previous section, phosphorous has an extremely rich phase diagram of unique complexity; at ambient conditions of pressure and temperature its three most common polymorphs, black-P, red-P and white-P are semiconducting or insulating. While black-P and red-P achieve metalization within a few GPa (estimating the exact value would require calculating corrections to the band-gap beyond DFT), white-P is still insulating at 7 GPa with a band gap of about 1.4 eV. Considering that DFT typically underestimates band gaps in insulators, this implies that white-P cannot be considered a candidate for the superconducting phase, and therefore will not be included in further investigations. Also red-P is excluded as a possible superconducting phase in the low-pressure range, because, although dynamically stable for 10 and 15 GPa, the calculated T_C is too low (< 1 K) to account for any experimental evidence of superconductivity. Upon further compression our calculations shown that red-P collapses to a simple cubic lattice. For black-P, on the contrary, the calculated T_C , depicted as black line in Fig. 1, rapidly increases as a function of pressure. This a consequence of the relatively strong electron-phonon coupling, which is consistent with previous predictions on doped black-P and phosphorene⁴⁴. This superconducting structure of black-P, which remains energetically *metastable* and dynamically stable for pressures up to 20 GPa, with transition temperatures as high as $\simeq 13$ K, is actually a modulated superstructure of the true black-P, obtained by supercell relaxation along soft directions. Upon further compression the modulated black-P relaxes to the simple cubic lattice.

However, at pressures in which superconductivity occurs (~ 10 GPa) the ground-state structure is not black-P, but A7-P, in good agreement with XRD measurements³⁷ and previous theoretical calculations⁴⁵. In this phase the calculated evolution of T_C is pressure-independent; T_C does remains constant ~ 7 K (red-line in bottom panel in Fig. 1). Noticeably, we find that the sudden increase in T_C for pressures above 20 GPa occurs in correspondence to the A7 \rightarrow *sc* second-order phase transition. Our calculations show that this substantial increase in T_C is not originated, as one could expect, from soft phonons inducing the structural transition which could consequently provide large electron-phonon coupling, but is instead triggered by an *electronic* Lifshitz transition⁴⁶. It does happen indeed that, upon increasing pressure, an additional band crosses the Fermi level, contributing to the electronic density of states (DOS) and providing a strong interband scattering channel that reinforces the Cooper pairing. An extensive analysis of this effect is provided in the Supplemental Material. The same behavior was recently predicted also in the superconducting properties of elemental sulfur under pressure⁴⁷, which remarkably has many common aspects with phosphorus.

Once the Lifshitz transition is completed, T_C marginally decreases with pressure as the occupation of the additional band increases, enhancing the electronic screening of the electron-phonon coupling. As a consequence T_C results rather featureless in the range between 40 to 100 GPa, where the only relevant phase is the *sc* one, showing T_C 's decreasing with pressure, in agreement with previous estimation⁴⁵. Considering only the thermodynamically stable structures, the predicted T_C follows closely the pressure dependence of the BCS-type coupling λ (Eq. 2), reported in Fig. 4 (blue curve in top panel). This is due to the combination of three factors: *first*, superconductivity is happening in the "weak-coupling limit", since the values of λ are between 0.4 and 0.7. In this limit T_C is extremely sensitive to λ . *Second*, the characteristic phonon energy scale ω_{og} (Eq. 3) and red line in the upper panel of Fig. 4) shows almost no pressure dependence, as would occur in presence of phononic instabilities. *Third*, the repulsive Coulomb interaction between electrons in the Cooper pairs, represented by the Coulomb pseudopotential parameter μ^* ^{48,49}, is constant and $\simeq 0.1$ for all structures and pressures, which is rather typical for *sp*-bonded systems. More insight on the pressure-evolution of the characteristic *ep* coupling parameters for the thermodynamically stable phases can be obtained analyzing the pressure evolution of the electron-phonon spectral function $\alpha^2F(\omega)$, shown in the bottom panel of Fig. 4. In the plot, frequencies are shown in ordinates, pressures in abscissas, and the color scale indicates the intensity of the $\alpha^2F(\omega)$; strongly-coupled phonons appear as darker regions at the corresponding frequencies. In general, the maximum phonon frequencies raise as pressure is increased. Up to around 20 GPa, the coupling is concentrated in the high-frequency modes, while the distribution changes at higher pressures (25–50 GPa) where it appears more evenly distributed. This means that, despite the pronounced hardening of the maximum phonon frequencies with pressure, the center of mass of the spectrum remains almost constant, and there are no signatures of lattice instabilities induced by electron-phonon coupling.

In contrast to the weak-coupling behavior of thermodynamically stable phases, *metastable* phases (black-P, *sc*, *sh* and *bcc*)

exhibit a marked strong-coupling behavior at the limit of their dynamical stability range. For these systems, upon approaching their structural transition, a considerable part of the phonon spectral weight is shifted to low frequencies, consequently increasing λ and a simultaneously decreasing ω_{log} . Further details, including the calculated $\alpha^2F(\omega)$, λ , ω_{log} and the Coulomb screening parameters for all phases discussed in this work can be found in the Supplemental Material.

High Pressures (50-350 GPa) We will now analyze the high-pressure range, for which our calculated T_C 's are summarized in the right bottom panel of Fig. 1. In the *sc* phase, T_C continues to decrease until the *sc* to *sh* transition occurs. Since this is a transition of first order, as the one from black-P to *sc*, we investigated the metastability of the two phases across their thermodynamic boundaries. For higher and lower pressures and for both systems our calculations predicts dynamically stable structures: *sc* up to 150 GPa and *sh* down to 80 GPa. Away from their thermodynamical phase boundaries, T_C varies rapidly in both systems and this is due to a phonon softening that lowers the phonon energy and increases the coupling. From 150 to 250 GPa, the T_C of *sh*-P decreases steadily below 3 K, and this phase is therefore moderately interesting for superconductivity. On the other hand, the *bccII* – 43*d* sequence of structures, stable above 250 GPa, is more promising. In fact, these phases show a larger T_C , well above 10 K. It is also worth mentioning that, between 220 and 250 GPa the *bcc* structure which is thermodynamically metastable, exhibits transition temperatures three times larger than those calculated for the *sh* structure.

Discussion

One of the crucial points of this work is to identify metastability as a distinctive feature of the phase diagram of phosphorus. In this element, the presence of several discontinuous phase transitions, not directly triggered by phononic instabilities, implies the coexistence of several metastable phases with distinct superconducting properties across the phase diagram. This means that the initial conditions and the $P - T$ path followed in the experiments largely determine the resulting crystal structure, coexistence of phases and the possibility of observing high- T_C metastable phases.

Using high-pressure experiments and first-principles calculations we are able to draw a consistent picture of the full phase diagram up to 350 GPa. We propose that the coexistence of two distinct superconducting phases of phosphorus in the 10–30 GPa pressure window successfully accounts for the the "anomalous" T_C vs. P trend first observed by Kawamura and coworkers⁵. Furthermore, we identified theoretically two other pressure regions in which superconducting T_C anomalies could be observed depending on the experimental conditions.

We first discuss the 10–30 GPa pressure interval, for which several experimental data are available. Here, we hypothesize that three phases actually play a role in the superconducting phase diagram, namely black-P, *R3m* and *sc*, and that the bifurcation in T_C seen by experiments is due to the coexistence the ground-state low- T_C A7-P and high- T_C metastable black-P phases, which both collapse to *sc* at $P \sim 20$ GPa. Our hypothesis perfectly accounts for the existing literature results of Kawamura *et al.*,⁵ in which the pressure cell was initially loaded with black-P, and pressure was subsequently increased either keeping the system at low temperature (Kawamura Path B in Fig. 1) – or following a room temperature path (Path A and C). The first experimental procedure leads to the highest T_C , and is remarkably well reproduced by calculations for black-P, while the second leads to a low T_C , and matches the calculated trend for A7 phosphorus.

The two new sets of experiments in this work were explicitly designed to reproduce the distinct T_C trends, and to test our interpretation in terms of A7 and black phosphorus. In contrast to previous experiments, in this work the cell was loaded with red-P at room temperature. In the first set (Exp. 1), the samples were kept at low temperatures during the whole pressure run. The first pressure measured was high enough (~ 5 GPa) to ensure a complete transition of red-P to black-P; according to our calculations, the transition should occur at ~ 2.5 GPa, and black-P should survive as a metastable phase for pressures well above 20 GPa, where it collapses to the *sc*. On the contrary, following the second path in the $P - T$ phase space (Exp. 2), where annealing cycles allow to reach the thermodynamically ground-state structures, will stabilize the A7 phase between 5 and ~ 20 GPa. Upon further compression the A7 structure will transform continuously to *sc* as our crystal prediction method confirmed. The measured T_C vs. P trends for the two paths closely reproduce the corresponding measurements of Kawamura *et al.*, and are in excellent agreement with our theoretical predictions, supporting our interpretation that the high- T_C phase is metastable black-P. An alternative explanation would be to ascribe the high T_C curve in Exp. 1 to a metastable red-P phase. We can safely rule out this hypothesis because, according to our calculations, after the metalization red-P has a negligible T_C (< 1 K).

It is worth to comment the recent measurements by Guo *et al.*⁷. They extend up to 50 GPa, and are generally consistent with previous measurements and ours, but seem to contradict our understanding of the low-pressure range. In fact, the authors report a gradual increase in T_C from 5 to 10 GPa followed by an abrupt jump, which does not have a straightforward interpretation. Our theoretical results suggest that a possible explanation for this phenomenon is the existence of a mixed black-P–*R3m* (O+R) phase (suggested by the same authors) which prevents a clear observation of the two distinct T_C trends, and is probably responsible for the oscillations in T_C observed up to ~ 25 GPa, where the samples enter to the *sc* phase and Guo's data merge with our measurements and older data.

Besides the low-pressure region already explored by Kawamura *et al.*, we predict two other ranges of pressure in which

different crystal structures are energetically accessible, and experimentally measurable: the first is around ~ 110 GPa, and a second is above ~ 220 GPa. In the first case, unfortunately the two competing phases have very similar critical temperatures (see T_C for *hex* and *sc* ~ 120 GPa), and are thus hard to distinguish experimentally. Moreover, phonons are softening close to the transition, coming both from low and high pressures, indicating that it could be difficult to stabilize metastable structures and that complex disordered or modulated structures may form⁵⁰. In the second case, the T_C 's of the ground-state and metastable structures (which according to our predictions is of comparable energetics at the relevant pressures) differ by a factor of three (see Fig. 3 and T_C 's for *sh*, *bcc* and *I-43d* above ~ 225 GPa). Therefore, these two distinct T_C vs. P trends should be easily discernible by experiments. However, no superconductivity measurements have been reported yet at these pressures, which was indeed unaccessible also for our current experimental setup. Nevertheless we note that, remarkably, our theoretical prediction of phase coexistence is consistent with recent XRD experiments³⁷. A possible path to achieve the synthesis of these metastable phases would be to start from the ground state structure at high pressures *I-43d* ($\lesssim 270$ GPa), cycle the sample through temperatures high enough to overcome the energetic barrier to the *sh* phase, and then cool the sample *slowly* releasing the pressure down to 230 GPa.

In summary, we have conducted a systematic theoretical and experimental investigation of elemental phosphorous under pressure. We have shown an excellent agreement between our experimental and theoretical results, which allow us not only to reconcile previous unexplained observed anomalies, but also to shed light onto the complex behavior of this element, which has the tendency to form many polymorphs and that differ substantially in their electronic and superconducting properties and can coexist in metastable forms in different pressure ranges. A similar behavior has been reported in a wide variety of conventional superconductors⁵¹, including simple elements⁵². The selective stabilization of metastable phases may represent, in the future, a viable strategy to improve the superconducting properties of conventional superconductors. For this, it is essential to assess the relative accuracy of experiments and calculations in this respect.

Methods

Crystal phase diagram exploration To sample the enthalpy landscape we employed the minima hopping method (MHM)⁵³ with unit cells of up to 8 atoms for selected pressures in the range of 0 to 350 GPa. This method has been successfully used for global geometry optimization in a large variety of applications^{54–58}, including superconducting materials at high pressure⁵⁶. The MHM was designed to thoroughly scan the low-lying enthalpy landscape of any compound and identify stable phases by performing consecutive short molecular dynamics escape steps followed by local geometry relaxations. The enthalpy surface is mapped out efficiently by aligning the initial molecular dynamics velocities approximately along soft-mode directions^{59,60}, thus exploiting the Bell-Evans-Polanyi⁶¹ principle to steer the search towards low energy structures. Energy, atomic forces and stresses were evaluated at the density functional theory (DFT) level with the Perdew-Burke-Ernzerhof (PBE)⁶² parametrization to the exchange-correlation functional. A plane wave basis-set with a high cutoff energy of 1000 eV was used to expand the wave-function together with the projector augmented wave (PAW) method as implemented in the Vienna Ab Initio Simulation Package VASP⁶³. Geometry relaxations were performed with tight convergence criteria such that the forces on the atoms were less than 2 meV/Å and the stresses were less than 0.1 eV/Å³. We have reproduced all the experimentally-known phases of P and other low-lying phases, except for white-P and red-P, for which larger supercell calculations are necessary to describe the structure.

Coupling and superconductivity calculations All superconductivity calculations are performed within Density Functional Theory for Superconductors (SCDFT)^{64,65}. The approximation used have been described in previous works^{14,18,47,66,67}. The pairing mechanism is due to the combined effect of electron-phonon coupling within DFT Kohn-Sham theory⁶⁸ as implemented in the QUANTUM ESPRESSO code, and electronic screening computed in the static random-phase-approximation⁶⁹. This allows us to calculate T_C completely *ab-initio*, without introducing any empirical parameter, such as the μ^* Coulomb pseudopotential usually used to solve the Eliashberg equations. Still, we can estimate an effective μ^* (reported in the Supplemental Material), fitting the fully *ab-initio* T_C with the Allen-Dynes-McMillan formula⁷⁰. The electron-phonon coupling at the Fermi energy is described in the isotropic approximation by the Eliashberg spectral functions⁴⁸, defined as:

$$\alpha^2 F(\omega) = \frac{1}{N_{E_F}} \sum_{\mathbf{k}, \mathbf{q}, \nu} |g_{\mathbf{k}, \mathbf{k}+\mathbf{q}, \nu}|^2 \delta(\epsilon_{\mathbf{k}}) \delta(\epsilon_{\mathbf{k}+\mathbf{q}}) \delta(\omega - \omega_{\mathbf{q}, \nu}), \quad (1)$$

where N_{E_F} is the DOS at the Fermi level, $\omega_{\mathbf{q}, \nu}$ is the phonon frequency of mode ν at wavevector \mathbf{q} and $|g_{\mathbf{k}, \mathbf{k}+\mathbf{q}, \nu}|$ is the electron-phonon matrix element between two electronic states with momenta \mathbf{k} and $\mathbf{k} + \mathbf{q}$. All computed $\alpha^2 F(\omega)$ are collected in Fig. 4. Anisotropy effects have been estimated to be irrelevant in the calculation of T_C and are neglected in this work. Two

significant moments of the Eliashberg function λ and ω_{log} , defined as:

$$\lambda = 2 \int \frac{\alpha^2 F(\omega)}{\omega} d\omega \quad (2)$$

$$\omega_{log} = \exp \left[\frac{2}{\lambda} \int \alpha^2 F(\omega) \frac{\ln(\omega)}{\omega} d\omega \right] \quad (3)$$

express, respectively, the electron-phonon coupling and the effective phononic energy.

Core atomic states are described in the norm-conserving pseudo-potential approximation; valence state are described by a plane-wave basis set with an energy cut-off 80 Ry. Since convergence checks have been performed independently on each phase, Brillouin zone integration is done with different sets of k -points in each crystalline structure, ranging from a minimum of 500 k -point per unit reciprocal volume (Bohr³) up to about 3,000 k -points per unit volume for electronic integration and about one fourth of this density for phononic sampling. The strict convergence criteria ensure that the numerical error in the solution of the SCDFE equations is small as compared to the intrinsic error-bar on the available functionals.

Experimental procedure High pressure electrical measurements were carried out using a diamond anvil cell (DAC) with an anvil tip diameter of 200–300 μ m bevelled at 7–8 degrees and with culet surface between 40–80 μ m. Four Ti electrodes were sputtered on the diamond anvil for the first experiment (Exp. 1) and three Ti electrodes for the second experiment (Exp. 2). The electrodes were capped with Au to prevent oxidation of the Ti (a zero contribution by the diamond surface to the conductivity was checked). An insulating gasket of Teflon was used to separate the metallic gasket from the electrodes. Red phosphorous was loaded in the DAC at ambient temperature and clamped at these conditions. The first pressure point after clamped was already about 3–5 GPa in both experiments. Then, the DAC was placed into a cryostat and cooled down to measure the first point of T_C at 13 GPa for the first experiment (Exp. 1) and 11 GPa for the second experiment (Exp. 2). The pressure was determined by a diamond edge scale at low temperatures using Raman spectra and we monitored any possible Raman signal from the samples. We used the 632.8 nm line of a He–Ne laser to excite the Raman spectra measured with a Raman spectrometer equipped with a nitrogen-cooled CCD and notch filters with resolution better than 2 cm^{−1}. Two different conditions were tested in our experiments, Exp. 1 and Exp. 2 as summarized in Fig. 2, with the only difference being the increased temperature at the beginning of the experiment. All the resistance measurements were done in increasing pressure; we could not perform measurements under decompression due to the diamond culet crack.

References

1. Drozdov, A. P., Eremets, M. I., Troyan, I. A., Ksenofontov, V. & Shylin, S. I. Conventional superconductivity at 203 kelvin at high pressures in the sulfur hydride system. *Nature* **525**, 2015/08/17/online (2015). DOI doi:10.1038/nature14964.
2. Mazin, I. I. Superconductivity: Extraordinarily conventional. *Nature* **525**, 40–41 (2015).
3. Eliashberg, G. Eliashberg Equations of Strong Coupling Theory. *Teor. Fiz* **38**, 966 (1960)[*Sov. Phys. FETP* **38** (1960).
4. Drozdov, A., Eremets, M. I. & Troyan, I. A. Superconductivity above 100 K in PH₃ at high pressures. *ArXiv e-prints* (2015). 1508.06224.
5. Kawamura, H., Shirogami, I. & Tachikawa, K. Anomalous superconductivity and pressure induced phase transitions in black phosphorus. *Solid state communications* **54**, 775–778 (1985).
6. Karuzawa, M., Ishizuka, M. & Endo, S. The pressure effect on the superconducting transition temperature of black phosphorus. *Journal of Physics: Condensed Matter* **14**, 10759 (2002).
7. Guo, J. *et al.* The vital role of hole-carriers for superconductivity in pressurized black phosphorus. *ArXiv e-prints* (2016). 1611.03330.
8. Troyan, I. *et al.* Observation of superconductivity in hydrogen sulfide from nuclear resonant scattering. *Science* **351**, 1303–1306 (2016).
9. Einaga, M. *et al.* Crystal structure of the superconducting phase of sulfur hydride. *Nature Physics* (2016).
10. Duan, D. *et al.* Pressure-induced metallization of dense (h₂s)₂h₂ with high-tc superconductivity. *Sci. Rep.* **4** (2014). DOI http://dx.doi.org/10.1038/srep06968.
11. Li, Y., Hao, J., Liu, H., Li, Y. & Ma, Y. The metallization and superconductivity of dense hydrogen sulfide. *The Journal of Chemical Physics* **140**, – (2014). URL <http://scitation.aip.org/content/aip/journal/jcp/140/17/10.1063/1.4874158>. DOI http://dx.doi.org/10.1063/1.4874158.

12. Bernstein, N., Hellberg, C. S., Johannes, M. D., Mazin, I. I. & Mehl, M. J. What superconducts in sulfur hydrides under pressure and why. *Phys. Rev. B* **91**, 060511 (2015). URL <http://link.aps.org/doi/10.1103/PhysRevB.91.060511>. DOI 10.1103/PhysRevB.91.060511.
13. Errea, I. *et al.* High-pressure hydrogen sulfide from first principles: A strongly anharmonic phonon-mediated superconductor. *Phys. Rev. Lett.* **114**, 157004 (2015). URL <http://link.aps.org/doi/10.1103/PhysRevLett.114.157004>. DOI 10.1103/PhysRevLett.114.157004.
14. Flores-Livas, A. J., Sanna, A. & Gross, E. High temperature superconductivity in sulfur and selenium hydrides at high pressure. *Eur. Phys. J. B* **89**, 1–6 (2016). URL <http://dx.doi.org/10.1140/epjb/e2016-70020-0>. DOI 10.1140/epjb/e2016-70020-0.
15. Ishikawa, T. *et al.* Superconducting h5s2 phase in sulfur-hydrogen system under high-pressure. *Scientific reports* **6** (2016).
16. Heil, C. & Boeri, L. Influence of bonding on superconductivity in high-pressure hydrides. *Phys. Rev. B* **92**, 060508 (2015). URL <http://link.aps.org/doi/10.1103/PhysRevB.92.060508>. DOI 10.1103/PhysRevB.92.060508.
17. Akashi, R., Sano, W., Arita, R. & Tsuneyuki, S. Possible “magnéli” phases and self-alloying in the superconducting sulfur hydride. *Phys. Rev. Lett.* **117**, 075503 (2016). URL <http://link.aps.org/doi/10.1103/PhysRevLett.117.075503>. DOI 10.1103/PhysRevLett.117.075503.
18. Flores-Livas, J. A. *et al.* Superconductivity in metastable phases of phosphorus-hydride compounds under high pressure. *Phys. Rev. B* **93**, 020508 (2016). URL <http://link.aps.org/doi/10.1103/PhysRevB.93.020508>. DOI 10.1103/PhysRevB.93.020508.
19. Shamp, A. *et al.* Decomposition Products of Phosphine Under Pressure: PH₂ Stable and Superconducting? *arXiv:1509.05455 [cond-mat]* (2015). URL <http://arxiv.org/abs/1509.05455>. ArXiv: 1509.05455.
20. Sakata, M., Nakamoto, Y., Shimizu, K., Matsuoka, T. & Ohishi, Y. Superconducting state of ca-vii below a critical temperature of 29 k at a pressure of 216 gpa. *Physical Review B* **83**, 220512 (2011).
21. Wigner, E. & Huntington, H. B. On the possibility of a metallic modification of hydrogen. *The Journal of Chemical Physics* **3**, 764–770 (1935). URL <http://scitation.aip.org/content/aip/journal/jcp/3/12/10.1063/1.1749590>. DOI <http://dx.doi.org/10.1063/1.1749590>.
22. Ashcroft, N. Metallic hydrogen: A high-temperature superconductor? *Phys. Rev. Lett.* **21**, 1748–1749 (1968). URL <http://link.aps.org/doi/10.1103/PhysRevLett.21.1748>. DOI 10.1103/PhysRevLett.21.1748.
23. Eremets, M., Troyan, I. & Drozdov, A. Low temperature phase diagram of hydrogen at pressures up to 380 gpa. a possible metallic phase at 360 gpa and 200 k. *arXiv preprint arXiv:1601.04479* (2016).
24. Dias, R. P. & Silvera, I. F. Observation of the wigner-huntington transition to metallic hydrogen. *Science* (2017). URL <http://science.sciencemag.org/content/early/2017/01/25/science.aal1579>. DOI 10.1126/science.aal1579. <http://science.sciencemag.org/content/early/2017/01/25/science.aal1579.full.pdf>.
25. Goncharov, A. F. & Struzhkin, V. V. Comment on observation of the wigner-huntington transition to metallic hydrogen. *arXiv preprint arXiv:1702.04246* (2017).
26. Loubeyre, P., Occelli, F. & Dumas, P. Comment on: Observation of the wigner-huntington transition to metallic hydrogen. *arXiv preprint arXiv:1702.07192* (2017).
27. Eremets, M. & Drozdov, A. Comments on the claimed observation of the wigner-huntington transition to metallic hydrogen. *arXiv preprint arXiv:1702.05125* (2017).
28. Brovman, E., Kagan, Y. & Kholas, A. Structure of metallic hydrogen at zero pressure. *Sov. Phys. JETP* **34**, 1300–1315 (1972).
29. Eremets, M. & Troyan, I. Conductive dense hydrogen. *Nature materials* **10**, 927–931 (2011).
30. Dalladay-Simpson, P., Howie, R. T. & Gregoryanz, E. Evidence for a new phase of dense hydrogen above 325 gigapascals. *Nature* **529**, 63–67 (2016).
31. Buzea, C. & Robbie, K. Assembling the puzzle of superconducting elements: a review. *Superconductor Science and Technology* **18**, R1 (2004).
32. Ruck, M. *et al.* Faserförmiger roter phosphor. *Angewandte Chemie* **117**, 7788–7792 (2005).
33. Hultgren, R., Gingrich, N. & Warren, B. The atomic distribution in red and black phosphorus and the crystal structure of black phosphorus. *The Journal of Chemical Physics* **3**, 351–355 (1935).

34. Akahama, Y., Kawamura, H., Carlson, S., Le Bihan, T. & Häusermann, D. Structural stability and equation of state of simple-hexagonal phosphorus to 280 gpa: Phase transition at 262 gpa. *Phys. Rev. B* **61**, 3139–3142 (2000). URL <http://link.aps.org/doi/10.1103/PhysRevB.61.3139>. DOI 10.1103/PhysRevB.61.3139.
35. Jamieson, J. C. Crystal structures adopted by black phosphorus at high pressures. *Science* **139**, 1291–1292 (1963).
36. Marqués, M. *et al.* Origin of incommensurate modulations in the high-pressure phosphorus iv phase. *Phys. Rev. B* **78**, 054120 (2008). URL <http://link.aps.org/doi/10.1103/PhysRevB.78.054120>. DOI 10.1103/PhysRevB.78.054120.
37. Sugimoto, T. *et al.* Identification of superlattice structure *ci16* in the p-vi phase of phosphorus at 340 gpa and room temperature via x-ray diffraction. *Phys. Rev. B* **86**, 024109 (2012). URL <http://link.aps.org/doi/10.1103/PhysRevB.86.024109>. DOI 10.1103/PhysRevB.86.024109.
38. Akahama, Y., Kobayashi, M. & Kawamura, H. Simple-cubic~simple-hexagonal transition in phosphorus under pressure. *Phys. Rev. B* **59**, 8520–8525 (1999). URL <http://link.aps.org/doi/10.1103/PhysRevB.59.8520>. DOI 10.1103/PhysRevB.59.8520.
39. Ehlers, F. J. H. & Christensen, N. E. Phosphorus under pressure: Ba-iv-type structure as a candidate for p-iv. *Phys. Rev. B* **69**, 214112 (2004). URL <http://link.aps.org/doi/10.1103/PhysRevB.69.214112>. DOI 10.1103/PhysRevB.69.214112.
40. Ishikawa, T., Nagara, H., Kusakabe, K. & Suzuki, N. Determining the structure of phosphorus in phase iv. *Phys. Rev. Lett.* **96**, 095502 (2006). URL <http://link.aps.org/doi/10.1103/PhysRevLett.96.095502>. DOI 10.1103/PhysRevLett.96.095502.
41. Fujihisa, H. *et al.* Incommensurate structure of phosphorus phase iv. *Phys. Rev. Lett.* **98**, 175501 (2007). URL <http://link.aps.org/doi/10.1103/PhysRevLett.98.175501>. DOI 10.1103/PhysRevLett.98.175501.
42. Katzke, H. & Tolédano, P. Displacive mechanisms and order-parameter symmetries for the *a7*-incommensurate-bcc sequences of high-pressure reconstructive phase transitions in group va elements. *Phys. Rev. B* **77**, 024109 (2008). URL <http://link.aps.org/doi/10.1103/PhysRevB.77.024109>. DOI 10.1103/PhysRevB.77.024109.
43. Boulfelfel, S. E., Seifert, G., Grin, Y. & Leoni, S. Squeezing lone pairs: The *a17* to *a7* pressure-induced phase transition in black phosphorus. *Phys. Rev. B* **85**, 014110 (2012). URL <http://link.aps.org/doi/10.1103/PhysRevB.85.014110>. DOI 10.1103/PhysRevB.85.014110.
44. Sanna, A. *et al.* First-principles and angle-resolved photoemission study of lithium doped metallic black phosphorous. *2D Materials* **3**, 025031 (2016). URL <http://stacks.iop.org/2053-1583/3/i=2/a=025031>.
45. Chan, K. T., Malone, B. D. & Cohen, M. L. Pressure dependence of superconductivity in simple cubic phosphorus. *Phys. Rev. B* **88**, 064517 (2013). URL <http://link.aps.org/doi/10.1103/PhysRevB.88.064517>. DOI 10.1103/PhysRevB.88.064517.
46. Lifshitz, I. Anomalies of electron characteristics of a metal in the high pressure region. *Journal of Experimental and Theoretical Physics* **11**, 1130 (1960). URL <http://www.jetp.ac.ru/cgi-bin/e/index/e/11/5/p1130?a=list>. Russian original - ZhETF, Vol. 38, No. 5, p. 1569, November 1960.
47. Monni, M., Bernardini, F., Sanna, A., Profeta, G. & Massidda, S. Origin of the critical temperature discontinuity in superconducting sulfur under high pressure. *Phys. Rev. B* **95**, 064516 (2017). URL <http://link.aps.org/doi/10.1103/PhysRevB.95.064516>. DOI 10.1103/PhysRevB.95.064516.
48. Allen, P. B. & Mitrović, B. *Theory of Superconducting T_c*, vol. 37 of *Solid State Physics* (Academic Press, 1983).
49. Morel, P. & Anderson, P. W. Calculation of the superconducting state parameters with retarded electron-phonon interaction. *Phys. Rev.* **125**, 1263–1271 (1962). URL <http://link.aps.org/doi/10.1103/PhysRev.125.1263>. DOI 10.1103/PhysRev.125.1263.
50. Marqués, M. *et al.* Origin of incommensurate modulations in the high-pressure phosphorus iv phase. *Phys. Rev. B* **78**, 054120 (2008). URL <http://link.aps.org/doi/10.1103/PhysRevB.78.054120>. DOI 10.1103/PhysRevB.78.054120.
51. Flores-Livas, J. A. *et al.* Enhancing the superconducting transition temperature of *bas_{i2}* by structural tuning. *Phys. Rev. Lett.* **106**, 087002 (2011). URL <http://link.aps.org/doi/10.1103/PhysRevLett.106.087002>. DOI 10.1103/PhysRevLett.106.087002.

52. Yin, Z. P., Gygi, F. & Pickett, W. E. Competing phases, strong electron-phonon interaction, and superconductivity in elemental calcium under high pressure. *Phys. Rev. B* **80**, 184515 (2009). URL <http://link.aps.org/doi/10.1103/PhysRevB.80.184515>. DOI 10.1103/PhysRevB.80.184515.
53. Goedecker, S. Minima hopping: An efficient search method for the global minimum of the potential energy surface of complex molecular systems. *The Journal of Chemical Physics* **120**, 9911 (2004).
54. Amsler, M. & Goedecker, S. Crystal structure prediction using the minima hopping method. *The Journal of Chemical Physics* **133**, 224104 (2010).
55. Amsler, M. *et al.* Crystal structure of cold compressed graphite. *Phys. Rev. Lett.* **108**, 065501 (2012). URL <http://link.aps.org/doi/10.1103/PhysRevLett.108.065501>. DOI 10.1103/PhysRevLett.108.065501.
56. Flores-Livas, J. A. *et al.* High-pressure structures of disilane and their superconducting properties. *Phys. Rev. Lett.* **108**, 117004 (2012). URL <http://link.aps.org/doi/10.1103/PhysRevLett.108.117004>. DOI 10.1103/PhysRevLett.108.117004.
57. Amsler, M. *et al.* Novel Structural Motifs in Low Energy Phases of LiAlH₄. *Phys. Rev. Lett.* **108**, 205505 (2012). URL <http://link.aps.org/doi/10.1103/PhysRevLett.108.205505>. DOI 10.1103/PhysRevLett.108.205505.
58. Botti, S., Flores-Livas, J. A., Amsler, M., Goedecker, S. & Marques, M. A. L. Low-energy silicon allotropes with strong absorption in the visible for photovoltaic applications. *Phys. Rev. B* **86**, 121204 (2012). URL <http://link.aps.org/doi/10.1103/PhysRevB.86.121204>. DOI 10.1103/PhysRevB.86.121204.
59. Roy, S., Goedecker, S., Field, M. J. & Penev, E. A Minima Hopping Study of All-Atom Protein Folding and Structure Prediction. *The Journal of Physical Chemistry B* **113**, 7315–7321 (2009).
60. Sicher, M., Mohr, S. & Goedecker, S. Efficient moves for global geometry optimization methods and their application to binary systems. *The Journal of Chemical Physics* **134**, 044106 (2011). URL <http://scitation.aip.org/content/aip/journal/jcp/134/4/10.1063/1.3530590>. DOI 10.1063/1.3530590.
61. Jensen, F. *Introduction to Computational Chemistry: Second Edition* (JW, 2011).
62. Perdew, J. P., Burke, K. & Ernzerhof, M. Generalized gradient approximation made simple. *Phys. Rev. Lett.* **77**, 3865–3868 (1996).
63. Kresse, G. & Furthmüller, J. Efficiency of ab-initio total energy calculations for metals and semiconductors using a plane-wave basis set. *Comput. Mat. Sci.* **6**, 15–50 (1996).
64. Oliveira, L. N., Gross, E. K. U. & Kohn, W. Density-functional theory for superconductors. *Phys. Rev. Lett.* **60**, 2430–2433 (1988). URL <http://link.aps.org/doi/10.1103/PhysRevLett.60.2430>. DOI 10.1103/PhysRevLett.60.2430.
65. Lüders, M. *et al.* Ab initio. *Phys. Rev. B* **72**, 024545 (2005). URL <http://link.aps.org/doi/10.1103/PhysRevB.72.024545>. DOI 10.1103/PhysRevB.72.024545.
66. Flores-Livas, J. A. & Sanna, A. Superconductivity in intercalated group-iv honeycomb structures. *Phys. Rev. B* **91**, 054508 (2015). URL <http://link.aps.org/doi/10.1103/PhysRevB.91.054508>. DOI 10.1103/PhysRevB.91.054508.
67. Linscheid, A., Sanna, A., Floris, A. & Gross, E. K. U. First-principles calculation of the real-space order parameter and condensation energy density in phonon-mediated superconductors. *Phys. Rev. Lett.* **115**, 097002 (2015). URL <http://link.aps.org/doi/10.1103/PhysRevLett.115.097002>. DOI 10.1103/PhysRevLett.115.097002.
68. Baroni, S., de Gironcoli, S., Dal Corso, A. & Giannozzi, P. Phonons and related crystal properties from density-functional perturbation theory. *Rev. Mod. Phys.* **73**, 515–562 (2001). URL <http://link.aps.org/doi/10.1103/RevModPhys.73.515>. DOI 10.1103/RevModPhys.73.515.
69. Massidda, S. *et al.* The role of coulomb interaction in the superconducting properties of cac 6 and h under pressure. *Superconductor Science and Technology* **22**, 034006 (2009). URL <http://stacks.iop.org/0953-2048/22/i=3/a=034006>.
70. Allen, P. B. & Dynes, R. C. Transition temperature of strong-coupled superconductors reanalyzed. *Phys. Rev. B* **12**, 905–922 (1975). URL <http://link.aps.org/doi/10.1103/PhysRevB.12.905>. DOI 10.1103/PhysRevB.12.905.

Acknowledgments

The authors acknowledge the hospitality of the *cini-Sardegna* meeting, where part of this work was written. J.A.F.-L. acknowledges computational resources under the project (s499 and s707) from the Swiss National Supercomputing Center (CSCS) in Lugano. A.D. and M.E acknowledge the European Research Council with the 2010-Advanced Grant 267777.

Author contributions statement

J.A.F.-L., A.S., L.B. and G.P. conceived the main idea of the research project. A.D. and M.E. performed the experiments. J.A.F.-L. and A.S. executed the ab-initio calculations. J.A.F.-L., A.S., A.D., L.B. and G.P. analyzed the results and wrote the manuscript. M.E. and S.G. reviewed the manuscript.

Additional information

The authors declare no competing financial interests.

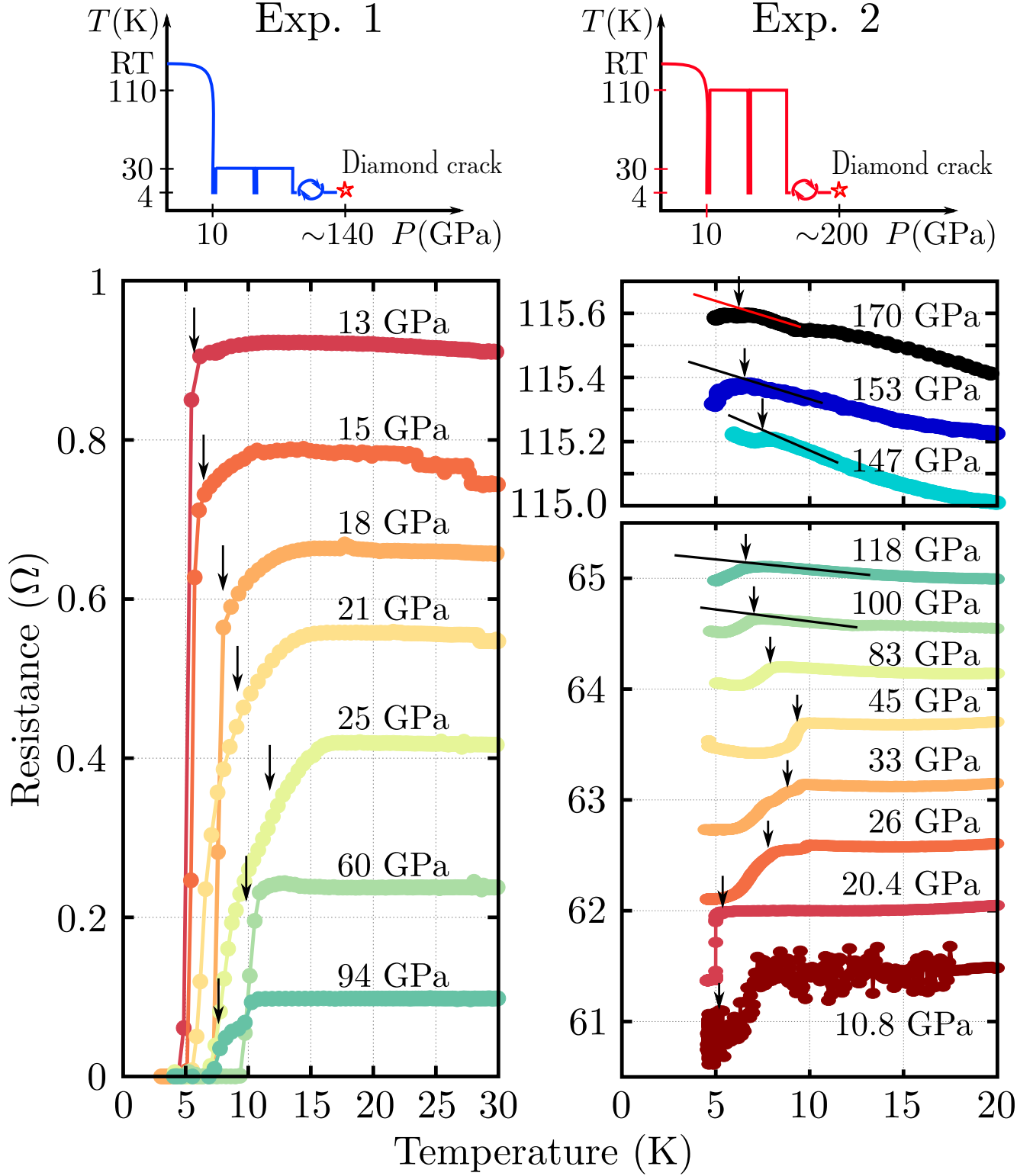


Figure 2. Bottom panels show resistivity measurements as a function of temperature for different pressures conditions: Exp. 1 (top-left panel) the sample was cycled at low temperature (< 30 K) and Exp. 2 (top-right panel) it was cycled up to high temperature (< 260 K). The T_C on-set for each pressure are marked with arrows. The corresponding values are summarized in Fig. 1.

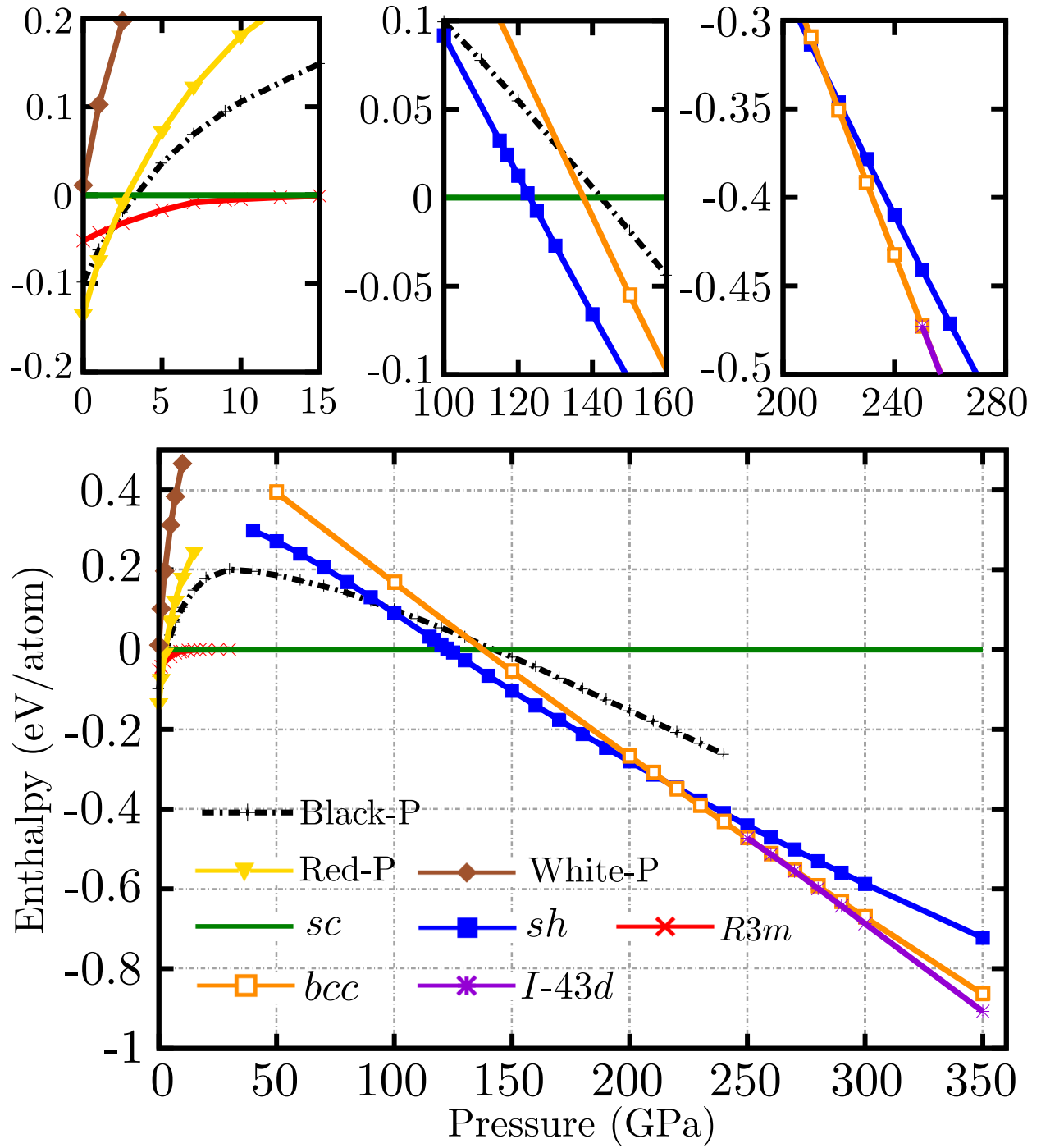


Figure 3. Calculated enthalpy for different crystal structures of phosphorus w.r.t *sc* as function of pressure. The top panels show an enlargement of three relevant pressure windows in which several structures are energetically competitive within orders of ~ 100 meV (left), ~ 15 meV (center) and ~ 5 meV (right).

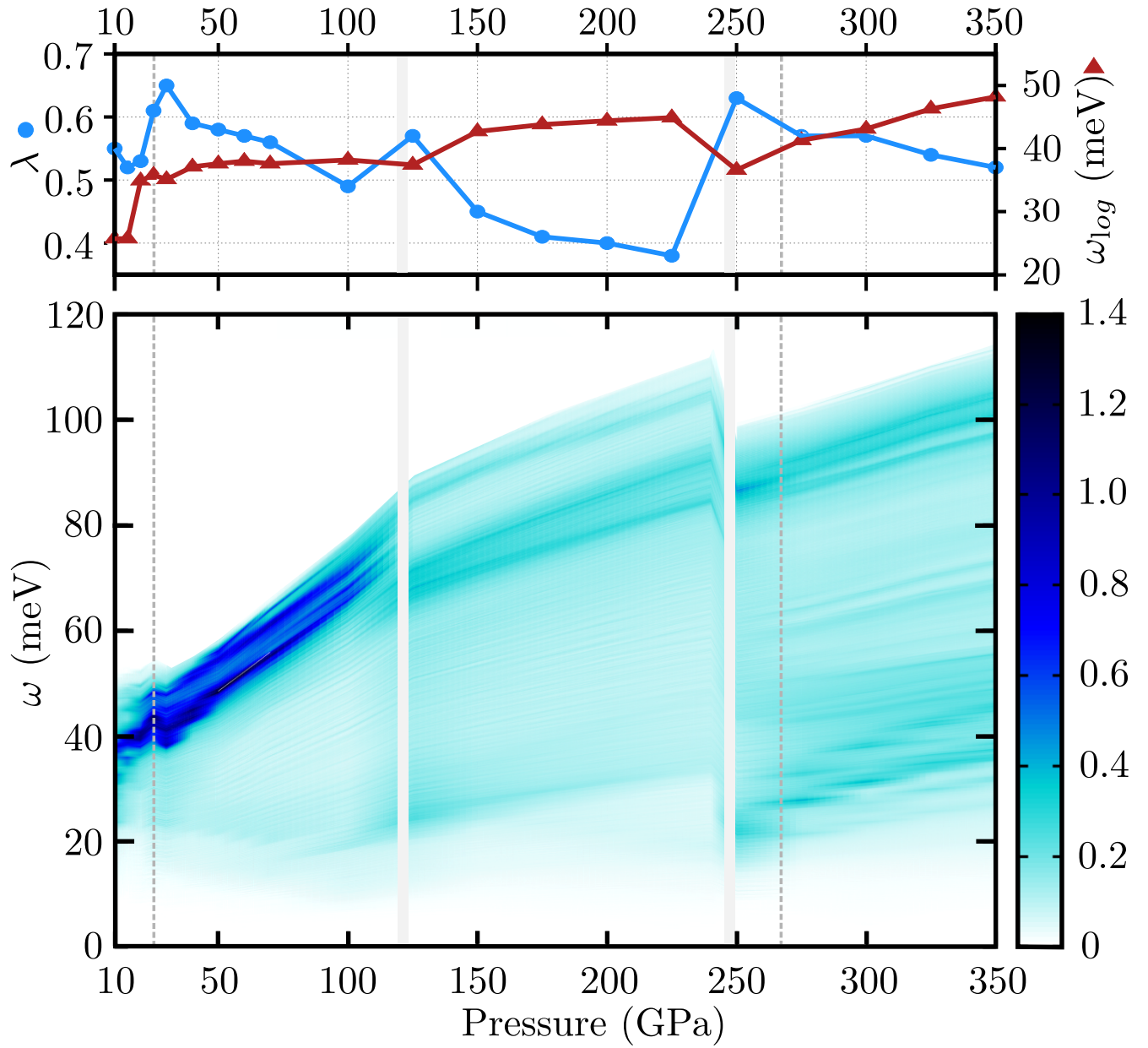


Figure 4. The bottom panel shows the pressure-evolution of the Eliashberg function $\alpha F^2(\omega)$ (Eq. 1), for all the thermodynamically stable phases of phosphorus between 10 and 350 GPa. Pressure are shown in abscissas, frequencies (ω) in ordinates; the function value is given by the color-scale. White vertical gaps mark first-order phase transition and gray dashed lines mark second-order transitions. The top panel shows the electron-phonon coupling constant λ (left y-axis) and the characteristic phonon energy ω_{\log} (right y-axis) obtained from the Eliashberg spectral functions. (see Methods and Supplemental Materials).